Constitutive modeling for compacted bentonite buffer materials as unsaturated and saturated porous media

Takayama, Yusuke
Tachibana, Shinya
Iizuka, Atsushi
Kawai, Katsuyuki
Kobayashi, Ichizo

(Citation)
Soils and Foundations,57(1):80-91

(Issue Date)
2017-02

(Resource Type)
journal article

(Version)
Version of Record

HOSTED BY
ELSEVIER
CrossMark
Available online at www.sciencedirect.com
ScienceDirect
Soils and Foundations 57 (2017) 80–91
SOILS AND FOUNDATIONS
www.elsevier.com/locate/sandf

Constitutive modeling for compacted bentonite buffer materials as unsaturated and saturated porous media

Yusuke Takayama [a,*], Shinya Tachibana [b], Atsushi Iizuka [b], Katsuyuki Kawai [c], Ichizo Kobayashi [d]

[a] *Japan Atomic Energy Agency, Japan*
[b] *Kobe University, Japan*
[c] *Kinki University, Japan*
[d] *Kajima Corporation, Japan*

Received 14 July 2015; received in revised form 26 September 2016; accepted 26 October 2016
Available online 10 February 2017

Abstract

Bentonite has remarkable swelling characteristics and low permeability that enhance the stability of the buffer materials in repositories for the geological disposal of radioactive waste. It is necessary to apply reliable numerical simulation techniques to assess the safety and mechanical stability of repositories over a long period of time. Having a constitutive model that can describe the mechanical behavior of bentonite is key to such numerical simulations. This paper proposes an elasto-plastic constitutive model to describe the changes in the mechanical properties of bentonite due to saturation in the progress of a repository becoming submerged under groundwater. In the proposed model, the swelling index is formulated as a function of the degree-of-saturation to express not only the swelling behavior, but also the dependency of the degree-of-saturation on the dilatancy characteristics. The montmorillonite content is used as a material parameter to determine the normal consolidation line. The experimental results of swelling volume and swelling pressure tests in previous literature are shown to have been satisfactorily predicted by the proposed model.

Keywords: Constitutive relations; Expansive soils; Numerical modeling; Stress analysis; Elastoplasticity (**IGC**: D05/D06/E14)

1. Introduction

Bentonite materials exhibit characteristics of high swelling and low permeability that make buffer materials suitable for use in repositories for the geological disposal of radioactive waste. Buffer materials are expected to act as self-sealing barriers to water channels, to prevent the leakage of radionuclide-contaminated groundwater, and to mitigate the stress caused by rock creep acting on the body of waste.

Bentonite buffer materials will be in an unsaturated condition as a result of compaction. After the closing of a repository, the bentonite materials will become saturated due to the seepage of groundwater. Reliable numerical simulations must therefore be developed in order to verify the long-term safety and mechanical stability of the compacted and unsaturated bentonite materials during their subsequent saturation. Having a constitutive model that can describe the mechanical behavior of bentonite in both unsaturated and saturated states is key to such numerical simulations.

To address the swelling characteristics of bentonite materials, various constitutive models have been proposed. Komine and Ogata (1996) proposed relational equations

Peer review under responsibility of The Japanese Geotechnical Society.
* Corresponding author.
E-mail address: takayama.yusuke@jaea.go.jp (Y. Takayama).

http://dx.doi.org/10.1016/j.sandf.2017.01.006
0038-0806/

for the swelling strain and swelling pressure of compacted bentonite based on the diffuse double-layer theory and showed the predictions of swelling test results with high accuracy. Namikawa et al. (2004) examined the applicability of some existing elasto-plastic constitutive models for non-expansive soil to saturated bentonite materials. Hirai and his colleagues (2005, 2006) presented an improved Cam-Clay model in an attempt to describe the mechanical behavior of saturated bentonite. Furthermore, various studies on the constitutive modeling of unsaturated bentonite have been done. The constitutive model proposed by Shuai and Fredlund (1998) expressed various swelling test results using an oedometer. Alonso and Gens (1999) proposed the Barcelona expansive model (BExM) to be used for the unsaturated state of expansive soil materials. By distinguishing micro-level void structures from macro-level ones, BExM expresses the mechanical behavior of unsaturated expansive soil. Sun and Sun (2012) highlighted the difficulty of applying BExM, especially with regard to parameter setting, and proposed an unsaturated constitutive model from a macroscopic perspective. Cui et al. (2002) proposed an unsaturated elastic constitutive model, in accordance with the concept of critical swelling curves, and simulated water absorption and swelling behavior under constant confining pressure, as well as compression behavior under constant suction conditions. Unsaturated constitutive models proposed by Oka et al. (2008) and Tachibana et al. (2012) expressed swelling behavior by adding new components of strain to the constitutive models that have been used for general clay materials.

On the other hand, in a study by Takayama et al. (2012), fundamental considerations of an elasto-plastic constitutive modeling for fully saturated bentonite were investigated. They examined the mechanical characteristics of bentonite based on recent experimental data taken from the literature. According to the results of triaxial CU tests on bentonite, conducted by Sasakura et al. (2002, 2003), Takaji and Suzuki (1999), and Ann et al. (2010), it was seen that the effective mean stress changed very little during shearing. This implies that bentonite possesses few dilatancy characteristics from the viewpoint of the critical state theory. In addition, converting the effective vertical stress obtained from oedometer tests into effective mean stress, using the relationship between the coefficient of earth pressure at rest (K0) and the over-consolidation ratio (OCR) obtained by Sasakura et al. (2003), it was found that the hysteresis response between loading and unloading processes scarcely appeared in the relationship between the void ratio and the effective mean stress. The behavior given by oedometer tests generally includes dilatancy behavior. However, because saturated bentonite has hardly any dilatancy characteristics, this relation can be considered as the isotropic loading and unloading response. Therefore, saturated bentonite can be regarded as a material in which the swelling line corresponds to the normal consolidation line (NCL).

Since there is no constitutive model for unsaturated bentonite which can express the mechanical behavior of saturated bentonite, a new constitutive model for unsaturated bentonite is proposed in this study. This study extends the elasto-plastic constitutive model for unsaturated non-expansive soil to that for bentonite materials. To verify the model's capability to represent the swelling and collapse behavior of bentonite materials, as seen in previous studies by Cui et al. (2004, 2006), simulations of swelling volume tests are performed. Furthermore, the swelling pressure is calculated using the proposed model to predict the experimental results obtained from the swelling pressure tests by Suzuki and Fujita (1999).

It should be noted that the present study focuses on the mechanical behavior of KuniGel V1, because repository designs in Japan currently suggest it as a candidate for bentonite buffer material. Moreover, since bentonite buffer materials in a repository will be in a compacted state and confined by the surrounding rock, the present study examines bentonite with a relatively high density. While KuniGel V1 is a bentonite clay composed mainly of montmorillonite, it also contains quartz, plagioclase, and other minor constituents. Table 1 shows the basic geotechnical properties of KuniGel V1 measured by Komine (2005). The montmorillonite content of KuniGelV1 produced before the year 2000 is 48%, but that after the year 2000 increases to 57%.

2. Constitutive modeling

According to Takayama et al. (2012), saturated bentonite possesses few dilatancy characteristics and the swelling line under the saturated condition corresponds to NCL. Moreover, it can be modeled as an elasto-plastic material in which plastic volumetric strain occurs to a very limited extent up to the critical state. In this section, a mechanical model for unsaturated bentonite, which takes into account these mechanical properties of saturated bentonite, is formulated by extending the effective degree of the saturation (*Se*)-hardening model proposed by Ohno et al. (2007), which is the elasto-plastic constitutive model for unsaturated non-expansive soil.

2.1. Se-hardening model for unsaturated soil

The *Se*-hardening model represents the mechanical characteristics and behavior of unsaturated soil such as

Table 1
Basic geotechnical properties of KuniGel V1 by Komine (2005).

Property	Before year 2000	After year 2000
Particle density (Mg/m^3)	2.79	2.79
Liquid limit (%)	473.9	458.1
Plastic limit (%)	26.61	23.7
Plasticity index	447.3	434.4
Montmorillonite content (%)	48	57

the increase in stiffness due to desaturation and collapses caused by water infiltration. Predictions of such typical behavior of unsaturated soil can be achieved by choosing not only the plastic volumetric strain, but also the effective degree of saturation as hardening parameters that control the size of the yield surface.

The effective stress under the unsaturated condition, proposed by Karube et al. (1996), is given by

$$\boldsymbol{\sigma}' = \boldsymbol{\sigma}^N + p_s\mathbf{1} \tag{1}$$

where $\boldsymbol{\sigma}'$: effective stress tensor; $\boldsymbol{\sigma}^N$: net stress tensor; p_s: suction stress; and $\mathbf{1}$: second order identity tensor. The net stress tensor and suction stress can be defined as

$$\boldsymbol{\sigma}^N = \boldsymbol{\sigma} - p_a\mathbf{1} \tag{2}$$

$$p_s = sS_e \tag{3}$$

where $\boldsymbol{\sigma}$: total stress tensor; p_a: pore air pressure; s: suction; and S_e: effective degree of saturation. Suction and the effective degree of saturation can be defined as

$$s = p_a - p_w \tag{4}$$

$$S_e = (S_r - S_{r0})/(1 - S_{r0}) \tag{5}$$

where p_w: pore water pressure; S_r: degree of saturation; and S_{r0}: residual degree of saturation at $s \to \infty$.

In the *Se*-hardening model, NCL is expressed as

$$e = e_0 - \lambda \ln \frac{p'}{p'_0} \tag{6}$$

where λ: compression index and e_0: void ratio corresponding to preconsolidation stress p'_0. The preconsolidation stress p'_0 in the unsaturated condition is expressed as a function of the effective degree of saturation S_e as follows:

$$p'_0 = \zeta p'_{sat0} \tag{7}$$

$$\zeta = \exp\{(1 - S_e)^n \ln a\} \tag{8}$$

where p'_{sat0}: preconsolidation stress corresponding to the void ratio of e_0 at the saturated state; and a, n: fitting parameters to determine the magnification of the preconsolidation stress in accordance with the effective degree of saturation ($1 \leqslant \zeta \leqslant a$). Fig. 1 shows the yield characteristics under the unsaturated condition. The normal consolidation line runs parallel to that of the saturated state ($S_e = 1.0$) with a decrease in the degree of saturation.

The yield function of the *Se*-hardening model is the same as that of the Cam-clay model and is expressed as

$$f(\boldsymbol{\sigma}', p'_c) = MD \ln \frac{p'}{p'_c} + D\frac{q}{p'} = 0 \tag{9}$$

where M: critical state parameter and p'_c: consolidation yield stress. Dilatancy coefficient D is defined as

$$D = \frac{\lambda - \kappa}{(1 + e_0)M} \tag{10}$$

where κ is a swelling index. Consolidation yield stress p'_c, which determines the size of the yield surface in an arbitrary unsaturated condition, is defined as

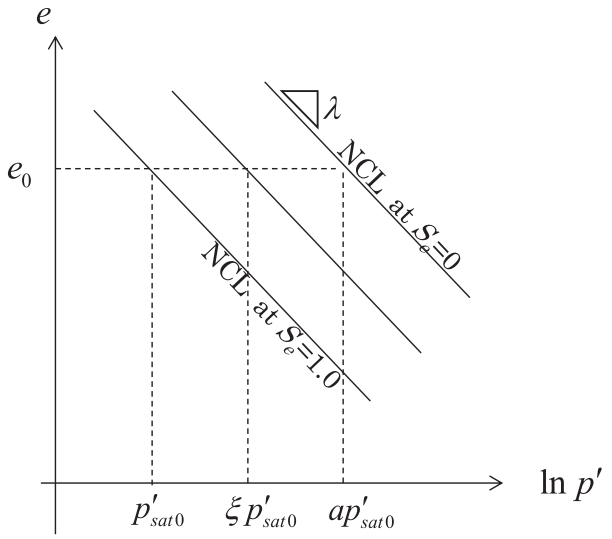

Fig. 1. Conceptual schematic of compression characteristics of unsaturated soil.

$$p'_c = \zeta p'_{sat} \tag{11}$$

where p'_{sat}: consolidation yield stress in a saturated condition. Fig. 2 shows a conceptual schematic of the yield surfaces. In the *Se*-hardening model, hardening occurs due to a decrease in the degree of saturation and the occurrence of plastic volumetric strain, while softening occurs due to an increase in the degree of saturation.

2.2. Extension of model to bentonite materials

2.2.1. Compression behavior of unsaturated bentonite materials

Kobayashi et al. (2007) determined the constant degree-of-saturation lines for a KuniGelV1 specimen through a series of one-dimensional air-drained and water-undrained compression tests with 35%, 30%, 25%, 20%, and 11% water contents until each specimen reached the saturated state. The constant degree-of-saturation lines obtained from these tests can be expressed as the following empirical equation:

$$\rho_d/\rho_w = 0.156 \ln \sigma_v - 0.77 \exp(-S_r/100/0.36) + 1.5 \tag{12}$$

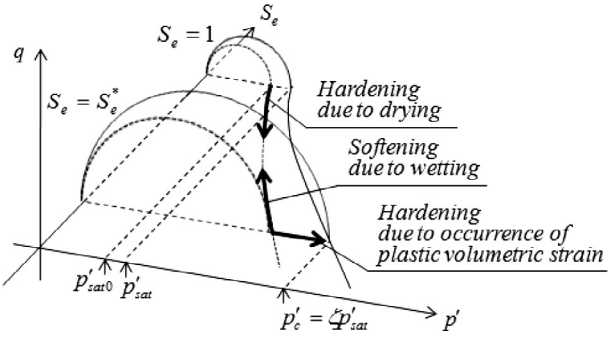

Fig. 2. Schematic of yield surfaces of Se-hardening model.

where ρ_d: dry density (Mg/m^3); ρ_w: water density (=1.0 Mg/m^3); and σ_v:vertical stress (MPa). Fig. 3 shows the constant degree-of-saturation lines drawn in the $e-\ln\sigma_v$ plane and illustrates that the constant degree-of-saturation lines in the $e-\ln\sigma_v$ plane are approximately parallel to one another. While Kobayashi et al. (2007) used the total stress rather than the effective stress to draw the constant degree-of-saturation lines, it would be appropriate to use the effective degree of saturation as a hardening parameter for bentonite under high pressure where the influence of suction is comparatively small, as modeled by Ohno et al. (2007). More specifically, in this model, the NCL is assumed as Eq. (6) and the swelling line of bentonite at a specific degree of saturation is assumed as

$$e = e|_{p'=p'_{sat}} - \kappa \ln \frac{p'}{\zeta p'_{sat}} \tag{13}$$

where $e|_{p'=p'_{sat}}$ is the void ratio at yield.

According to Takayama et al. (2012), the swelling line substantially corresponds to the normal consolidation line only when the bentonite becomes saturated. Compression index λ and swelling index κ, therefore, have the following relations:

$$\kappa \approx \lambda \quad \text{when} \quad S_r = 1.0 \tag{14}$$

$$\kappa < \lambda \quad \text{when} \quad S_r < 1.0 \tag{15}$$

Moreover, since the constant degree-of-saturation lines are subparallel, as shown in Fig. 3, compression index λ is independent of the degree of saturation, while swelling index κ depends on the degree of saturation.

2.2.2. Modeling of dilatancy characteristics

Based on the above-mentioned interpretation proposed by Takayama et al. (2012), saturated bentonite possesses few dilatancy characteristics. On the other hand, the results of constant volume direct shear tests under the unsaturated condition conducted by Kodaka and Teramoto (2009) show that unsaturated bentonite possesses dilatancy characteristics. Thus, the plastic volume changes due to shear under saturated and unsaturated conditions are expressed as the following two equations, respectively.

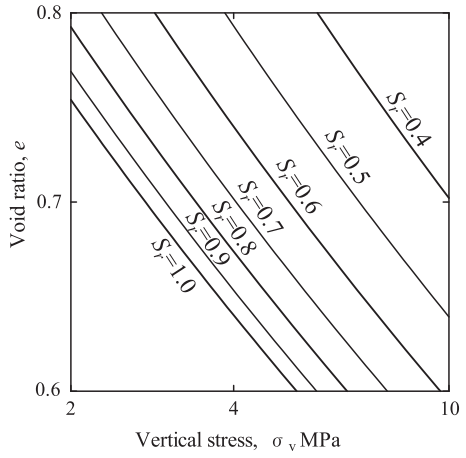

Fig. 3. Constant degree-of-saturation lines of KuniGel V1 proposed by Kobayashi et al. (2007).

$$\varepsilon_v^p \approx 0 \text{ when } S_r = 1.0 \tag{16}$$

$$\varepsilon_v^p \neq 0 \text{ when } S_r < 1.0 \tag{17}$$

Eq. (16) predicts almost no change in the elastic volume change ($\varepsilon_v^e \approx 0$) under constant volume shear only under the saturated condition, and brings a glacial change in the effective mean stress through a hypo-elastic constitutive relation, as specified in Section 2.3. Such expressions of dilatancy characteristics can be attained by introducing the dependency of the degree of saturation on the swelling index, as shown in Eqs. (14) and (15), since the present study describes the plastic volumetric strain in a similar formulation to the *Se*-hardening model or the Cam clay model as

$$\varepsilon_v^p = \frac{\lambda-\kappa}{1+e_0} \ln \frac{p'}{p'_0} + D\frac{q}{p'} \tag{18}$$

Based on the assumption that critical state parameter M is constant and independent of the degree of saturation, Eq. (18) encompasses both Eqs. (16) and (17) via the definition of dilatancy coefficient in Eq. (10) only by modeling the swelling index so as to satisfy Eqs. (14) and (15). In other words, such treatment of the swelling index enables the model to express the volume changes due to not only the swelling, but also the shearing in a wider range of degrees of saturation. This idea for the swelling index in the constitutive modeling comes from careful observations of the typical and qualitative behavior of bentonite. It would be impossible to explicitly determine the relationship between the swelling index and the degree of saturation through the experiment results. Thus, in this study, an evolutional law for the swelling index is proposed as a monotone increasing function according to the increase in the degree of saturation.

$$\kappa = \kappa(S_r) = \kappa_0 - (\kappa_0 - \kappa_{sat})S_e^l \tag{19}$$

where κ_{sat} is the swelling index at the saturated condition which should be slightly smaller than compression index λ; κ_0: swelling index at $S_e = 0$; and $l(>0)$: fitting parameter that controls the dependency of the degree of saturation. It is noted that, if $\kappa_{sat} = \kappa_0$ is set, the swelling index becomes independent of the degree of saturation and the model is reduced to the *Se*-hardening model. Figs. 4 and 5, for example, show the dependence on the swelling index and the dilatancy coefficient of the effective degree of saturation, respectively, with the values of $\lambda = 0.125$, $\kappa_0 = 0.010$, $e_0 = 0.10$, and $M = 0.45$.

Fig. 6 shows conceptual schematics of a state boundary surface and an elastic wall at (a) unsaturated and (b) saturated states determined by the model proposed in the present study. The state boundary surface in the volume

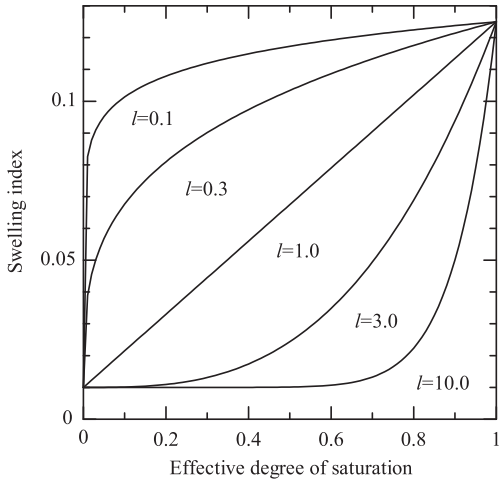

Fig. 4. Changes in swelling index with changes in effective degree of saturation.

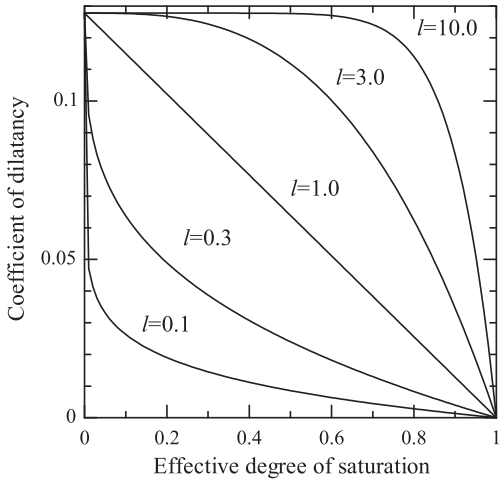

Fig. 5. Changes in coefficient of dilatancy with changes in effective degree of saturation.

constant section ($e = e_0$) at an unsaturated state is ζ-times as large as that at a saturated state in the direction of the p'-axis, as specified in Eq. (7), while it deforms into an upward convex shape along the q-axis in accordance with the approach of the swelling index to the compression index due to saturation, as defined in Eq. (19). Therefore, the shape of the state boundary strongly depends on the degree of saturation. On the other hand, the yield surface which is a projection of the intersection between an elastic wall and a state boundary surface on the $p' - q$ plane just expands due to hardening or shrinks due to softening in a similar fashion to the *Se*-hardening model without any change in shape since the proposed model characterizes a single critical state line and the shape of the yield surface depends only upon critical state parameter M. It is noted that, if the associated flow rule is applied to this model, the increment in plastic volumetric strain becomes zero at the critical state.

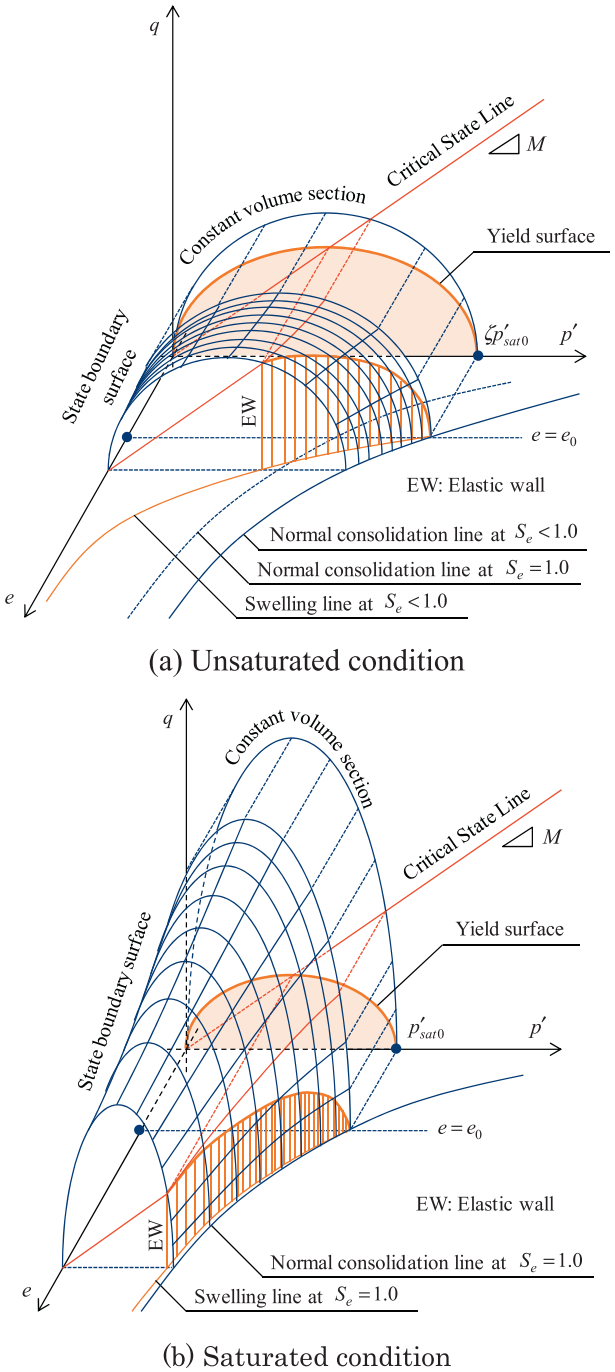

Fig. 6. Conceptual schematic of state surfaces and swelling walls.

2.2.3. *Effect of montmorillonite content on NCL of saturated bentonite*

Kobayashi et al. (2011) examined several factors that influence the NCL of bentonite, such as the types of interlayer cation and the montmorillonite content, and pointed out the importance of the montmorillonite content in determining the consolidation characteristics of bentonite. Based on the study by Kobayashi et al. (2011), the montmorillonite content is used here as a material parameter to characterize the location of the normal consolidation

line in the $e - \ln p'$ plane at a saturated state for various bentonite materials.

Fig. 7 shows the results of oedometer tests on saturated bentonite material with various montmorillonite contents conducted by Takaji and Suzuki (1999), Ishikawa et al. (1997), Sasakura et al. (2002), and Ishibashi et al. (2011). It can be seen from this figure that the smaller the montmorillonite content, the lower the position of the normal consolidation line will be. In order to specify the location of each normal consolidation line, the values of the vertical effective stress corresponding to the void ratio of 0.65 are plotted against the montmorillonite content in Fig. 8 together with a fitting curve determined by the least squares method, as the following formula:

$$\sigma'|_{e=0.65} = 0.14\exp(0.06\alpha_{mon}) \tag{20}$$

where $\sigma'|_{e=0.65}$: vertical effective stress (in MPa) corresponding to the void ratio of 0.65 and α_{mon}: montmorillonite content (%). The void ratio of 0.65, which is almost equivalent to the dry density of 1.6 Mg/m^3, is selected on the grounds that this value is a candidate for dry density in the design of bentonite buffers suggested by the Japan Nuclear Cycle Development Institute (2000).

Here, it is assumed that the NCL for saturated bentonite can be described by

$$e = e_{ref} - \lambda \ln \frac{p'}{p'_{ref}} \tag{21}$$

where e_{ref}: reference void ratio and p'_{ref}: reference stress in terms of the mean effective stress (MPa). According to the experimental data obtained by Sasakura et al. (2003), the coefficient of earth pressure at rest remains at almost 1.0 under the normal compression process. It is therefore assumed that effective vertical stress σ'_v, in Figs. 7 and 8, is equal to mean effective stress p'. Reference void ratio e_{ref} and reference stress p'_{ref} in Eq. (21) can be expressed as

$$e_{ref} = 0.65 \tag{22}$$

$$p'_{ref} = 0.14\exp(0.06\alpha_{mon}) \tag{23}$$

Fig. 9 shows a conceptual schematic of the compression and swelling characteristics in the proposed model.

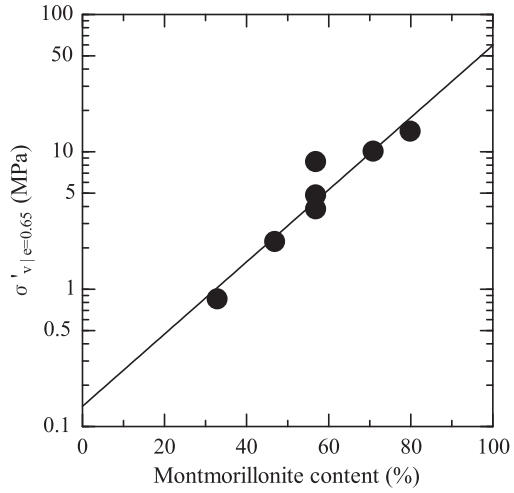

Fig. 8. Relationship between montmorillonite content and vertical stress at void ratio of 0.65.

2.3. Incremental form of elasto-plastic stress-strain relation

The increment in the elastic volumetric strain can be written as

$$\dot{\varepsilon}^e_v = -\frac{\dot{e}}{1+e_0} \tag{24}$$

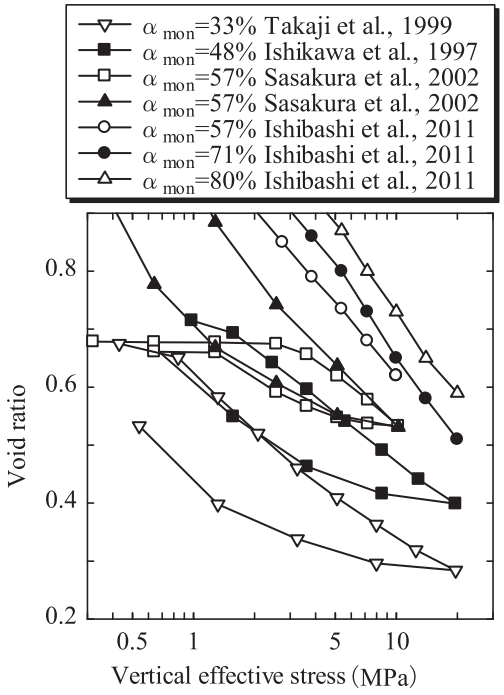

Fig. 7. Results of oedometer tests on saturated bentonite with various montmorillonite contents.

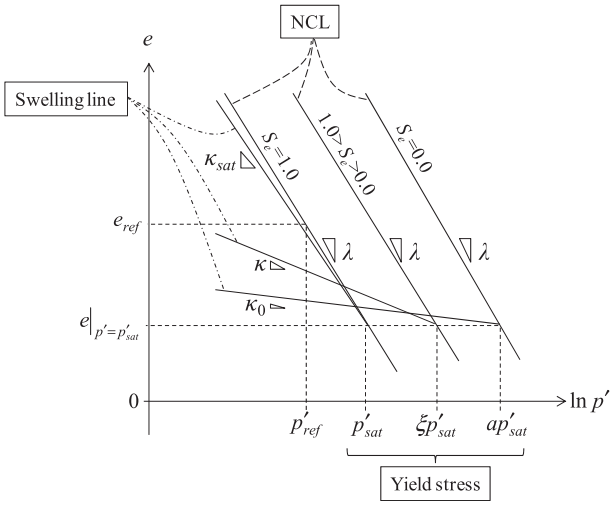

Fig. 9. Conceptual schematic of compression and expansion characteristics in proposed model.

By substituting Eq. (13) together with Eqs. (8) and (19) into Eq. (24), the isotropic part of the incremental stress-strain relation under the elastic condition can be developed as

$$\dot{p}' = K\dot{\varepsilon}_v^e + K_{S_e}\dot{S}_e \tag{25}$$

where elastic moduli K and K_{S_e} are, respectively, expressed as

$$K = \frac{1+e_0}{\kappa_0 - (\kappa_0 - \kappa_{sat})S_e^l}p' \tag{26}$$

$$K_{S_e} = \frac{(\kappa_0 - \kappa_{sat})lS_e^{l-1}\ln\frac{p'}{\zeta p'_{sat}} - [\kappa_0 - (\kappa_0 - \kappa_{sat})S_e^l]n(1-S_e)^{n-1}\ln a}{\kappa_0 - (\kappa_0 - \kappa_{sat})S_e^l}p' \tag{27}$$

The following nonlinear and hypo-elastic constitutive relation, which contains Eq. (25), is applied in this study:

$$\dot{\boldsymbol{\sigma}}' = \mathbf{C}^e : \dot{\boldsymbol{\varepsilon}}^e + K_{S_e}\dot{S}_e\mathbf{1} \tag{28}$$

noting that

$$\mathbf{C}^e = K\mathbf{1}\otimes\mathbf{1} + 2G\mathbf{A} \tag{29}$$

$$G = \frac{3(1-2\nu')}{2(1+\nu')}K \tag{30}$$

$$\mathbf{A} = \mathbf{I} - \frac{1}{3}\mathbf{I}\otimes\mathbf{I} \tag{31}$$

where G: elastic shear modulus; ν': effective Poisson's ratio; and $\mathbf{I}$: fourth order identity tensor.

The yield function of the proposed model can be expressed as

$$f(\boldsymbol{\sigma}', S_e, p'_{sat}) = \frac{\lambda - \kappa(S_e)}{1+e_0}\ln\frac{p'}{\zeta p'_{sat}} + D\frac{q}{p'} = 0 \tag{32}$$

It is noted that dilatancy coefficient D is also a function of the degree of saturation via Eq. (10). In order to derive the incremental elasto-plastic stress-strain relation, the consistency condition of Eq. (32) is applied as

$$\dot{f}(\boldsymbol{\sigma}', S_e, p'_{sat}) = \frac{\partial f}{\partial \boldsymbol{\sigma}'} : \dot{\boldsymbol{\sigma}}' + \frac{\partial f}{\partial S_e}\dot{S}_e + \frac{\partial f}{\partial p'_{sat}}\dot{p}'_{sat} = 0 \tag{33}$$

where the differential operators can be obtained as follows:

$$\frac{\partial f}{\partial \boldsymbol{\sigma}'} = \frac{MD}{3p'}\left[1 - \left(\frac{q}{p'M}\right)\right]\mathbf{1} + \frac{3D}{2qp'}\mathbf{s} \tag{34}$$

$$\frac{\partial f}{\partial S_e} = \frac{(\kappa_0 - \kappa_{sat})lS_e^{l-1}}{1+e_0}\left[\ln\frac{p'}{p'_{sat}\exp[(1-S_e)^n\ln a]} + \frac{q}{p'M}\right] + \frac{\lambda - \kappa_0 + (\kappa_0 - \kappa_{sat})S_e^l}{1+e_0}(1-S_e)^{n-1}n\ln a \tag{35}$$

$$\frac{\partial f}{\partial p'_{sat}} = -\frac{MD}{p'_{sat}} \tag{36}$$

The hardening law can be characterized in a similar form to the Se-hardening model as

$$\frac{\dot{p}'_{sat}}{p'_{sat}} = \frac{\dot{\varepsilon}_v^p}{MD} \tag{37}$$

It is assumed here that the increment in plastic strain $\dot{\boldsymbol{\varepsilon}}^p$ can be determined by the associated flow rule.

$$\dot{\boldsymbol{\varepsilon}}^p = \gamma\frac{\partial f}{\partial \boldsymbol{\sigma}'} \tag{38}$$

where γ: plastic multiplier. Based on the assumption that the increment in strain is decomposed into elastic and plastic components, the strain increment can be represented as

$$\dot{\boldsymbol{\varepsilon}} = \dot{\boldsymbol{\varepsilon}}^e + \dot{\boldsymbol{\varepsilon}}^p \tag{39}$$

The substitution of Eqs. (38) and (39) into Eq. (28) yields

$$\dot{\boldsymbol{\sigma}}' = \mathbf{C}^e : \left(\dot{\boldsymbol{\varepsilon}} - \gamma\frac{\partial f}{\partial \boldsymbol{\sigma}'}\right) + K_{S_e}\dot{S}_e\mathbf{1} \tag{40}$$

Plastic multiplier γ can be obtained by substituting Eq. (40) into the consistency condition of Eq. (33) as

$$\gamma = \frac{\frac{\partial f}{\partial \boldsymbol{\sigma}'} : \mathbf{C}^e : \dot{\boldsymbol{\varepsilon}} + \left[\frac{\partial f}{\partial p'}K_{S_e} + \frac{\partial f}{\partial S_e}\right]\dot{S}_e}{\frac{\partial f}{\partial \boldsymbol{\sigma}'} : \mathbf{C}^e : \frac{\partial f}{\partial \boldsymbol{\sigma}'} + \frac{\partial f}{\partial p'}} \tag{41}$$

where

$$\frac{\partial f}{\partial p'} = \frac{MD}{p'}\left[1 - \frac{q}{p'M}\right] \tag{42}$$

substituting Eq. (41) into Eq. (40), the incremental form of the elasto-plastic stress-strain relation can be formulated as

$$\dot{\boldsymbol{\sigma}}' = \left[\mathbf{C}^e - \frac{\mathbf{C}^e : \frac{\partial f}{\partial \boldsymbol{\sigma}'}\otimes\frac{\partial f}{\partial \boldsymbol{\sigma}'} : \mathbf{C}^e}{\frac{\partial f}{\partial \boldsymbol{\sigma}'} : \mathbf{C}^e : \frac{\partial f}{\partial \boldsymbol{\sigma}'} + \frac{\partial f}{\partial p'}}\right] : \dot{\boldsymbol{\varepsilon}} - \left[\frac{\mathbf{C}^e : \frac{\partial f}{\partial \boldsymbol{\sigma}'}\left(\frac{\partial f}{\partial p'}K_{S_e} + \frac{\partial f}{\partial S_e}\right)}{\frac{\partial f}{\partial \boldsymbol{\sigma}'} : \mathbf{C}^e : \frac{\partial f}{\partial \boldsymbol{\sigma}'} + \frac{\partial f}{\partial p'}} - K_{S_e}\mathbf{1}\right]\dot{S}_e \tag{43}$$

In the simulations carried out in the next chapter, Eq. (43) will be solved simultaneously with the soil-water retention characteristic model by imposing the prescribed conditions. The loading condition in each step will be judged by the sign of the plastic multiplier.

3. Performance of proposed constitutive model

In order to verify the proposed constitutive model, swelling volume and swelling pressure tests have been simulated. The swelling volume test measures the volume changes of the bentonite, whereby the bentonite is allowed to absorb water under a constant confining pressure. In contrast, the swelling pressure test ascertains the pressure developing in the bentonite due to water absorption under a constant volume condition. These tests should be treated as boundary value problems rather than element-wise tests because bentonite samples typically exhibit heterogeneous distributions of density and degree-of-saturation during the tests. However, the samples used in these experiments are sufficiently small. Hence, the present study reasonably assumes that the sample keeps its uniformity and that the

state at all stages of swelling is isotropic. The present study conducts the simulations by using the constitutive relation in order to verify its capability to predict the swelling behavior of bentonite. In these simulations, the soil-water retention characteristic curve (SWRCC) model proposed by Kawai et al. (2002) is applied; it incorporates the logistic curve formula derived by Sugii and Uno (1996).

The logistic curve is formulated as

$$S_r = S_{ra} + (S_{rf} - S_{ra})/(1 + s^B \exp A) \tag{44}$$

In the SWRCC model, parameters A and B are input individually for each of the wetting and drying processes from the current state: $s = s^*$ and $S_r = S_r^*$. Thus, the lower limit of degree of saturation S_{ra} for the wetting curve and the upper limit of degree of saturation S_{rf} for the drying curve are, respectively, determined as follows:

$$\left.\begin{aligned} A = A^W, B = B^W, S_{rf} = 1.0, \quad \text{and} \\ S_{ra} = \frac{S_r^*(1+s^{*B}\exp A) - S_{rf}}{s^{*B}\exp A} \end{aligned}\right\} \quad \text{for the wetting curve} \tag{45}$$

$$\left.\begin{aligned} A = A^D, B = B^D, S_{ra} = S_{r0}, \quad \text{and} \\ S_{rf} = S_{ra} + (S_r^* - S_{ra})(1 + s^{*B}\exp A) \end{aligned}\right\} \quad \text{for the drying curve} \tag{46}$$

3.1. Simulation of swelling volume tests

Simulations of the swelling volume tests on the bentonite material with the montmorillonite content of 48% are carried out in order to verify the responses from two types of initial conditions, namely, the normally consolidated state (Case 1) and the over-consolidated state (Case 2), while both cases assume the same initial values for suction and the degree of saturation. Tables 2 and 3 summarize the initial conditions and the material parameters, respectively, used in the simulations. Fig. 10 shows the soil-water retention curves applied in the simulation. The values for κ_0, a, n, l, and the parameters in the SWRCC model are all assumed. Actually, while the behavior of the bentonite under the unsaturated condition can be modeled from the viewpoints of unsaturated soil mechanics and careful analyses of the reliable but limited experimental data, it is next to impossible to explicitly determine the parameters related to the unsaturated condition since it is somewhat difficult even to measure the matric suction of the bentonite with a relatively lower degree of saturation.

Table 2
Initial conditions for simulation of swelling volume tests.

	Case 1	Case 2
Initial total mean stress (MPa)	4.41	4.41
Initial effective mean stress (MPa)	4.89	4.89
Initial void ratio	0.78	0.49
Initial degree of saturation	0.50	0.50
Initial suction (MPa)	1.09	1.09

Table 3
Material parameters used in simulation.

Compression index, λ	0.14
Swelling index at $S_e = 0$, κ_0	0.01
Montmorillonite content, α_{mon} (%)	48
Specific gravity, G_s	2.79
Fitting parameter, l	10
Se-hardening model parameter, a	20
Se-hardening model parameter, n	1
Parameter for SWRCC, A^W (for kPa)	−11
Parameter for SWRCC, B^W	1.6
Parameter for SWRCC, A^D (for kPa)	−37
Parameter for SWRCC, B^D	4.2
Residual degree of saturation, S_{r0}	0.1

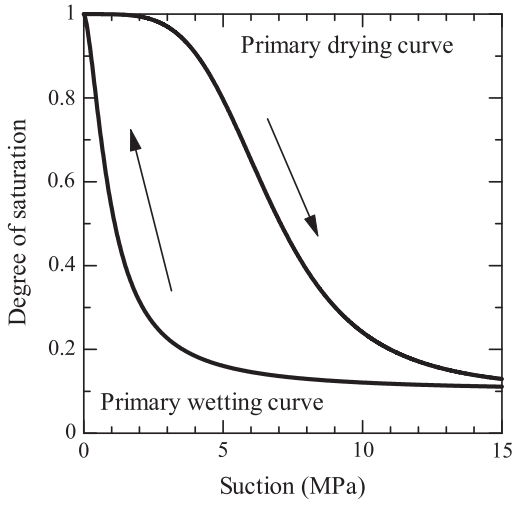

Fig. 10. Soil-water retention characteristic curves.

Therefore, this kind of parameter should be estimated through the inverse analyses of boundary value problems, such as one-dimensional infiltration tests, static compaction tests, and swelling tests. However, it is noted that the primary motivation for this simulation is to examine the functions of the proposed model for expressing the typical swelling behavior of bentonite. Determining the parameters and comparing the numerical and the experiment results are research tasks for future studies.

Fig. 11 shows the changes in void ratio, effective mean stress, and suction stress for Cases 1 and 2 with a monotonic increase in the degree of saturation. In both cases, the total mean stress is set to be constant and the suction changes along the same wetting curve from the same initial point. In Case 1, the void ratio decreases with an increase in the degree of saturation, whereas the void ratio increases in Case 2. This difference between Cases 1 and 2 is caused by the balance of plastic compression and elastic expansion. In Case 1, the plastic compression is dominant, whereas the elastic expansion is dominant in Case 2. Although this tendency can be originally predicted by the Se-hardening model, the large elastic expansion with a decrease in the effective mean stress in Case 2 occurs due to the increase in swelling index, as modeled in this study.

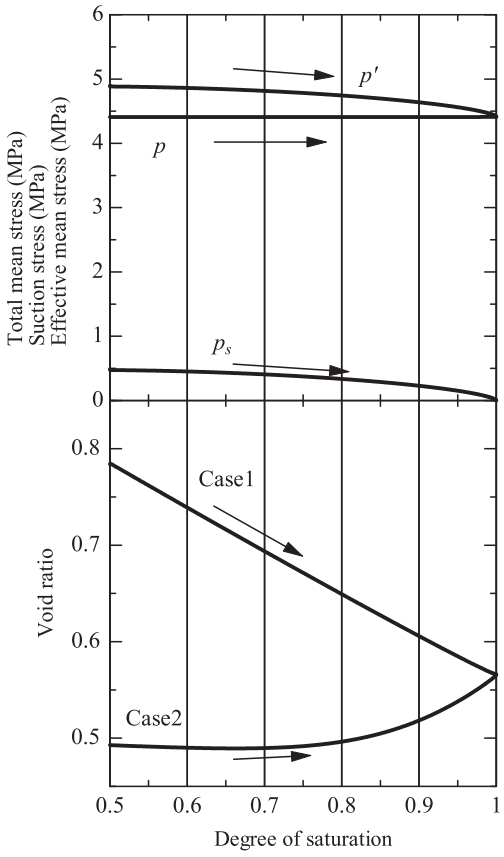

Fig. 11. Changes in effective mean stress, suction stress, and void ratio calculated in simulations of swelling volume tests.

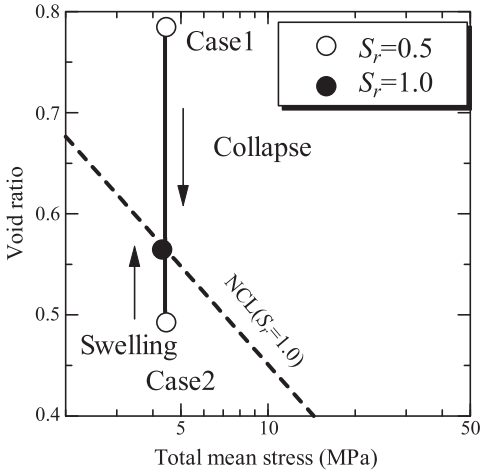

Fig. 12. Relationship between void ratio and total mean stress in swelling process.

Fig. 12 shows the relationship between the void ratio and the total stress, while Fig. 13 shows the relationship between the void ratio and the effective stress. These figures illustrate that the void ratio in both Cases 1 and 2 reaches the same point at the saturated state in spite of the initial void ratio being different. Cui et al. (2004, 2006) carried out a series of swelling volume tests and suggested the existence of a unique relationship between the void ratio and

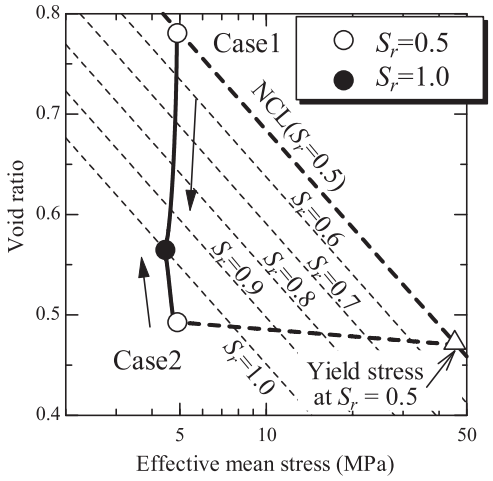

Fig. 13. Relationship between void ratio and effective mean stress in swelling process.

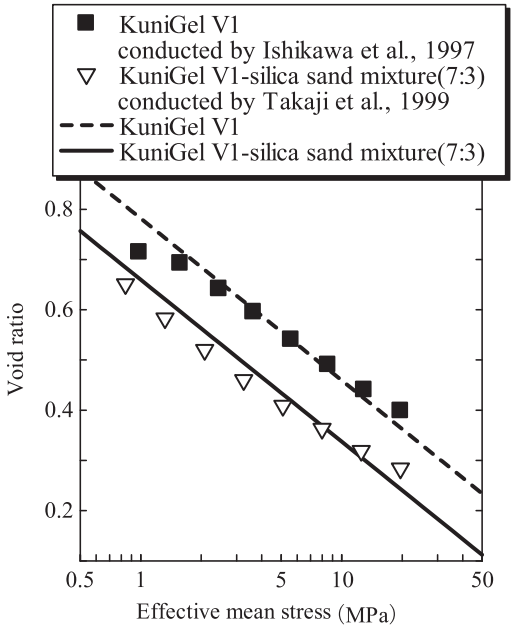

Fig. 14. NCL at saturated state applied in simulations of swelling pressure tests.

the confining pressure at the saturated state. This implies that the looser and unsaturated bentonite initially above the correlation line, between the confining pressure and the void ratio, contracts due to water infiltration, while the denser and unsaturated bentonite below the correlation line expands. The model proposed in the present study can express such typical behavior, as suggested by Cui et al. (2004, 2006).

3.2. Simulation of swelling pressure test

The responses of swelling pressure tests on two materials, namely, KuniGel V1 and a KuniGel V1-silica sand mixture at a ratio of 7:3, were simulated. The input parameters are

Table 4
Analysis cases.

	Case 1	Case 2	Case 3	Case 4
Initial effective mean stress (MPa)	0.47	0.47	0.47	0.47
Initial total mean stress (MPa)	0	0	0	0
Initial void ratio	0.80	0.70	0.60	0.50
Initial degree of saturation	0.70	0.70	0.70	0.70
Initial suction (MPa)	0.70	0.70	0.70	0.70

the same as those shown in Table 3, except for montmorillonite content of the KuniGel V1-silica sand mixture of 33.6%. It is noted that the calculated value for the swelling pressure at the saturation state is independent of the SWRCC and the values of κ_0, a, n, and l because the effective mean stress reaches the nearby NCL when saturated (see Fig. 6). The NCL assumed in this simulation is shown in Fig. 14. Table 4 shows the analysis cases. Four cases were simulated by setting different values for the void ratio. Fig. 15(a) and (b) show changes in the total stress, the effective stress, and the suction stress with an increase in the degree of saturation. As the initial total stress is set to zero, it is appropriate to regard the total stress in Fig. 15 (a) and (b) as the swelling pressure. It can be seen from these figures that the swelling pressure increases monotonously with an increase in the degree of saturation. Moreover, in cases with smaller void ratios, higher swelling pressures are calculated. For the same void ratio, the silica sand mixture provides a lower swelling pressure than KuniGel V1. Fig. 16 shows the relationship between the void ratio and the effective mean stress for Case 4 in the simulation of the swelling pressure test on KuniGel V1. The initial point

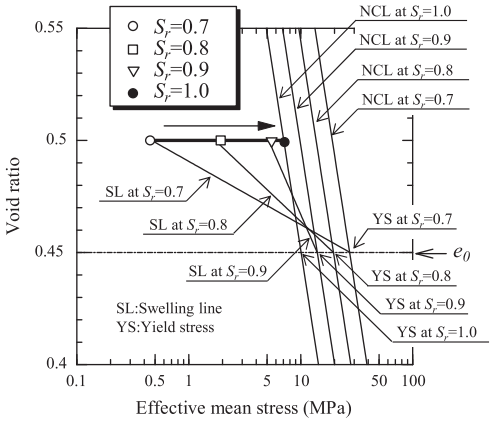

Fig. 16. Relationship between void ratio and effective mean stress of Case 4 in simulations of swelling pressure tests on KuniGel V1.

exists on the swelling line at Sr = 0.7. The void ratio is constant at the value of 0.5 during swelling and the effective mean stress is increased in accordance with the approach of the swelling index to the compression index due to saturation, as defined in Eq. (19). The saturation point reaches the vicinity of the NCL at Sr = 1.0. Fig. 17(a) and (b) show the relationship between swelling pressure and the dry density at the saturated state, as well as the results of the swelling pressure test on KuniGel V1 and the silica sand mixture conducted by Suzuki and Fujita (1999). The calculated swelling pressure at the saturated state tends to increase with the increase in dry density and is in satisfactory agreement with the test results from Suzuki and Fujita (1999). However, in some cases, the proposed model slightly overestimated the

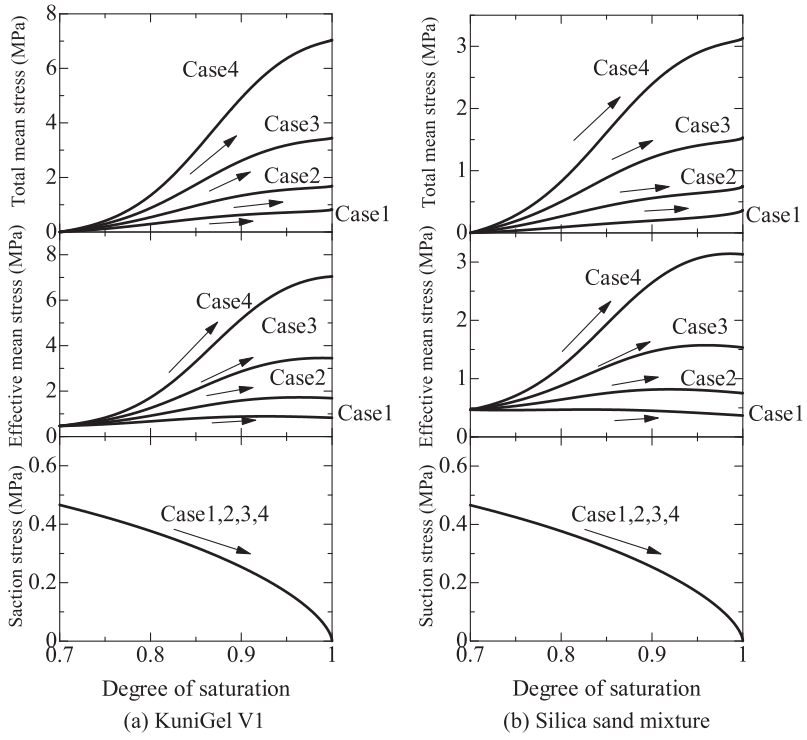

Fig. 15. Changes in total mean stress, effective mean stress, and suction stress calculated in simulations of swelling pressure tests.

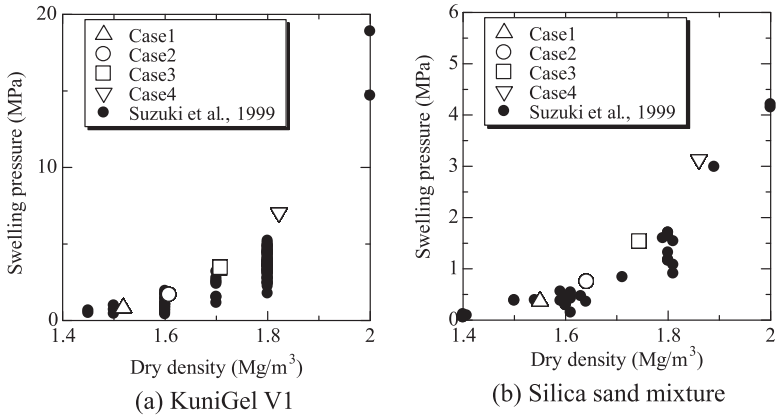

Fig. 17. Relationship between dry density and swelling pressure at saturated state.

data. The experimental data show the variability in the swelling pressure even if the dry density is the same. It is necessary, therefore, to give further consideration from the viewpoint of boundary value problems.

4. Conclusion

It is necessary to develop a reliable constitutive model to assess the safety and mechanical stability of repositories over a long period of time. In this paper, therefore, a new constitutive model has been proposed to predict the mechanical behavior of unsaturated and saturated bentonite. The findings of the present study are summarized below:

- In the proposed model, the swelling index and the dilarancy coefficient in the Cam-clay model or the Se-hardening model have been formulated as a function of the degree-of-saturation.
- The model is applicable to bentonite materials with various values of montmorillonite content because the montmorillonite content is used as a material parameter.
- In order to verify the capability of the model to express the swelling behavior of unsaturated bentonite, simulations of swelling volume tests were performed. The simulation results showed that the model could satisfactorily express the collapse behavior of the initially looser bentonite and the volume expansion of the initially dense one.
- An element simulation of swelling pressure tests was performed. The simulation results were in agreement with the test results for two bentonite materials, namely, KuniGel V1 and a KuniGel V1-silica sand mixture.

References

Alonso, E.E., Gens, A., 1999. Modelling the mechanical behaviour of expansive clays. Eng. Geol. 21, 173–183.

Ann, D., Lennart, B., Lars-Erik, J., 2010. Stress-Strain Relation of Bentonite at Undrained Shear. SKB Technical Report TR-10-32.

Cui, H., Sun, D., Matsuoka, H., 2006. Swelling characteristics of Sand-Bentonite mixtures under isotropic and anisotropic stress states. J. Geotech. Eng. 62 (3), 657–666 (in Japanese).

Cui, H., Sun, D., Matsuoka, H., Yongfu, X.U., 2004. Swelling characteristics of Sand-Bentonite mixtures under one-dimensional stress. J. Geotech. Eng. 67 (3), 275–285 (in Japanese).

Cui, Y.J., Yahia-Aissa, M., Delage, P., 2002. A model for the volume change behavior of heavily compacted swelling clays. Eng. Geol. 64, 233–250.

Hirai, T., Shigeno, Y., Iizuka, A., 2005. An elasto-plastic constitutive modeling for swelling buffer materials. J. Appl. Mech. 8, 395–402 (in Japanese).

Hirai, T., Shigeno, Y., Takaji, K., Iizuka, A., 2006. Study on constitutive model of elastoplastic behavior for swelling buffer material. J. Appl. Mech. 9, 471–478 (in Japanese).

Ishibashi, N., Komine, H., Yasuhara, K., Murakami, S., Mori, T., Ito, H., 2011. Influence of montmorillonite content on consolidation characteristics of Bentonite. 46th Japan National Conference on Geotechnical Engineering, Japan (in Japanese).

Ishikawa, H., Ishiguro, K., Namikawa, T., Sugano, T., 1997. Consolidation Properties of Buffer Material. PNC TN8410 97-051 (in Japanese).

Japan Nuclear Cycle Development Institute, 2000. H12: Project to Establish the Scientific and Technical Basis for HLW Disposal in Japan. JNC TN1400 99-020 (in Japanese).

Karube, D., Kato, S., Hamada, K., Honda, M., 1996. The relationship between the mechanical behavior and the state of porewater in unsaturated soil. J. JSCE 34 (535), 83–92 (in Japanese).

Kawai, K., Wang, W., Iizuka, A., 2002. The expression of hysteresis appearing on water characteristic curves and the change of stresses in unsaturated soils. J. Appl. Mech. 5, 777–784 (in Japanese).

Kobayashi, I., Owada, H., Ishii, T., 2011. Hydraulic/mechanical modeling of smectitic materials for HMC analytical evaluation of the long term performance of TRU geological repository. Proceedings of the 14th International Conference on Environmental Remediation and Radioactive Waste Management, ICEM2011-59090, France.

Kobayashi, I., Toida, M., Sasakura, T., Ohta, H., 2007. Interpretation of compression/swelling behavior of compacted bentonite using constant water-content line and constant degree-of saturation line. J. Geotech. Eng. 63 (4), 1065–1078 (in Japanese).

Kodaka, T., Teramoto, Y., 2009. Shear failure properties of compacted bentonite under unsaturated and saturated conditions. Jpn. Geotech. J. 4 (1), 59–69 (in Japanese).

Komine, H., Ogata, N., 1996. Prediction for swelling characteristics of compacted bentonite. Can. Geotech. J. 33, 11–22.

Komine, H., 2005. Influence of production year of the same bentonite on applicability of a theoretical evaluation model to swelling characteristics. Proc. Annual Meeting of JSCE (in Japanese).

Namikawa, T., Hirai, T., Tanai, K., Yui, M., Shigeno, Y., Takaji, K., Ohnuma, M., 2004. Study on applicability of elasto-viscoplastic models to mechanical properties of compacted bentonite. J. Geotech. Eng. 67 (764), 367–372 (in Japanese).

Ohno, S., Kawai, K., Tachibana, S., 2007. Elasto-plastic constitutive model for unsaturated soil applied effective degree of saturation as a parameter expressing stiffness. J. JSCE 63 (4), 1132–1141 (in Japanese).

Oka, F., Feng, H., Kimoto, S., Higo, Y., 2008. An elasto-viscoplastic numerical analysis of swelling process of un-saturated bentonite. J. Appl. Mech. 11, 369–376.

Sasakura, T., Kuroyanagi, M., Okamoto, M., 2002. Studies on Mechanical Behavior of Bentonite for Development of the Constitutive Model. JNC TJ8400-2002-025 (in Japanese).

Sasakura, T., Kuroyanagi, M., Kobayashi, I., Okamoto, M., 2003. Studies on Mechanical Behavior of Bentonite for Development of the Constitutive Model II. JNC TJ8400 2003-048 (in Japanese).

Shuai, F., Fredlund, D.G., 1998. Model for the simulation of swelling-pressure measurements on expansive soils. Can. Geotech. J. 35, 96–114.

Sugii, T., Uno, T., 1996. Modeling of hydraulic properties for unsaturated soils. Proc. Symp. Permeability of Unsaturated Ground, Japan, pp. 179–184 (in Japanese).

Sun, W., Sun, D., 2012. Coupled modelling of hydro-mechanical behaviour of unsaturated compacted expansive soils. Int. J. Numer. Anal. Meth. Geomech. 36, 1002–1022.

Suzuki, H., Fujita, T., 1999. Swelling Characteristics of Buffer Material. JNC TN8400 99-038 (in Japanese).

Tachibana, S., Takayama, Y., Iizuka, A., Kawai, K., Ohno, S., Kobayashi, I., 2012. Elasto-plastic constitutive model for expansive soils with a concept of fully saturation curve. Proc. 5th Asia-Pacific Conf. on Unsaturated Soils, Thailand, pp. 325–330.

Takayama, Y., Tsurumi, S., Iizuka, A., Kawai, K., Ohno, S., 2012. An interpretation of mechanical properties of bentonite as a non-linear elastic material. Int. J. GEOMATE 3, 357–362.

Takaji, K., Suzuki, H., 1999. Static Mechanical Properties of Buffer Material. PNC TN8400 99-041 (in Japanese).